STUDY ON HEAT TRANSFER CHARACTERISTICS OF HONEYCOMB LIQUID-COOLED LITHIUM BATTERY MODULE

by

Yaxin SUN and Kequn LI*

College of Energy and Power Engineering,
University of Shanghai for Science and Technology, Shanghai, China

Original scientific paper
https://doi.org/10.2298/TSCI211123030S

To ensure that a lithium battery can operate in the appropriate temperature range, the 18650-type lithium battery (cylindrical battery with diameter of 18 mm and height of 65 mm) was selected as the research object, and the thermal model of single battery was established. Compared with reference values, the data correlate well and the accuracy of the model is validated. The liquid-cooling model of a honeycomb lithium battery module was established based on a thermal model of a single battery. By using numerical simulation, the coolant flow rate, coolant temperature and central angle of coolant channel are set as variables to analyze the heat transfer characteristics of the battery module at different ambient temperature. The results show that increasing the flow rate and the central angle of the coolant channel can improve the temperature homogeneity. Compared with the flow rate, the central angle has a greater effect on the heat transfer characteristics. The coolant temperature has a significant effect on the temperature distribution of the battery module. However, the temperature homogeneity is deteriorated.

Key words*: lithium battery, battery thermal management, liquid cooling, temperature distribution*

Introduction

Due to relatively economical and effective mining, transportation and storage, fossil energy is the main energy in China, and coal is the cheapest and largest source of energy in China [1]. Recently, global warming, environmental pollution and the energy crisis have become increasingly prominent. To reduce fossil energy consumption, most countries are leaning towards the development of electric vehicles [2]. Many nations have taken steps to ban the sale of passenger vehiceles powered by fossil fuels. Lithium batteries have received wide attention because of their high energy density, long service life and low self-discharge rate [3] which made it the mainstream power supply in electric vehicle [4]. However, the performance of lithium batteries is closely related to the operating temperature. During discharging and charging, a large amount of heat is generated because of the internal resistance effect and the polarisation reaction in the battery [5]. Heat accumulation will cause the battery's temperature to rise and the temperature difference to increase, causing capacity

*Corresponding author, e-mail: kequn_li@126.com

decay, and thermal runaway of the battery. Furthermore, adverse operating conditions, such as rapid charging, undesirable climate and battery ageing, can also cause excessive heat production. According to existing research, the appropriate operating temperature range of a lithium battery is between 298 K and 313 K, and the appropriate internal temperature difference is less than 5 K [6, 7]. Excessive or low temperatures will have a greater impact on its performance, lifecycle, and safety [3]. Lithium batteries must be connected in series or in parallel to form battery modules. The performance degradation of single batteries will inevitably affect the performance of the entire battery pack [8]. Therefore, it is critical to develop a cooling system with excellent performance and capable of analysing its heat transfer characteristics for the safe, reliable and efficient operation of electric vehicles [9].

Existing battery thermal management system technology includes air [10], liquid [11], phase change [12], heat pipe [13], and mixed cooling [14]. Air cooling is considered the simplest and cheapest method, but due to its low thermal conductivity and low heat capacity, it still has limitations in some extreme conditions [15]. Phase change materials absorb or release a large amount of heat when phase change occurs. Under severe conditions, they have better temperature control than air forced convection [16-19]. However, phase change materials have poor thermal conductivity in single phase. The cooling efficiency of heat pipe is high, but the effect on temperature homogeneity is general. At the same time, the complex heat pipe structure cannot match the battery well, and the volume of the whole battery system will be increased. In addition, heat pipe cooling also has the disadvantages of high manufacturing cost, complex installation and reduced heat transfer performance after long-term use. Mixed cooling can effectively overcome the shortcomings of single heat management technology and achieve better heat management effect, but the mixed way increases the quality and structure of heat management system. It is necessary to formulate the corresponding thermal management strategy according to the specifications and operating environment of the battery pack and in combination with economic benefits. Because of the excellent cooling effect of liquid media, liquid cooling has better heat transfer performance than other methods, and can keep the temperature within an appropriate range while maintaining a smaller temperature difference [20**,** 21].

Chen *et al*. [15] found that the indirect liquid cooling system has the lowest temperature rise and is more practical than direct liquid cooling by comparing the cooling modes of different Li-ion battery packs. Jin *et al*. [22] used a liquid-cooling plate with oblique ribs in the micro-channel. The resulting fluid self-disturbance enhances the heat transfer capacity of the cooling plate. Researches [23-25] investigated the influence of the number of channels, flow direction, flow velocity, and ambient temperature on the thermal behavior of battery packs through numerical simulation for three micro-channel liquid-cooling schemes. Basu *et al*. [26] simulated the micro-channel liquid-cooling method of an 18650 nickel-cobalt-aluminum ternary lithium battery pack and verified the effectiveness of its cooling scheme. Zhao *et al*. [27] established a thermal model of 71 18650-type lithium batteries to simulate and study the effect of the discharge rate, cooling fluid flow rate and the contact area between the battery and outer wall of the liquid-cooling channel on the thermal behavior of the battery pack. Most of the aforementioned studies focus on the research of plate liquid cooling battery module, but the cooling effect is not very ideal due to the limited contact area with the battery. An *et al*. [28] used ethylene glycol as a cooling liquid and analysed its effect on the maximum temperature and temperature difference of the honeycomb battery pack. However, the arrangement of the coolant channel results in a small contact area with the battery, and the heat exchange effect is not ideal. Feng *et al*. [29] proposed a honeycomb liquid-cooled battery module and studied the charging and discharging temperature changes of the battery pack at different ambient temperatures through experiments. Because of the single-inlet-outlet structure, as the coolant flows, its heat exchange effect weakens. It takes a long time for the temperature of the battery module to reach a stable and appropriate range.

In this study, a honeycomb liquid-cooled lithium battery module is proposed. Select 18650-type lithium battery as the research object because 18650-type lithium batteries are the mainstream power battery of electric vehicles and the selected 18650-type lithium batteries are the same as those in [30]. The coolant mini-channel is indirectly and closely surround each battery, which increases the contact area between the liquid cooling channel and batteries. Meanwhile each battery exchanges heat with the coolant separately, avoiding the situation that the cooling effect of a single-inlet-outlet structure decreases with the flow of coolant, shorten the time required for cooling or heating. In addition, the whole module is simple and compact. Based on the thermal model of single lithium battery, a 3-D transient model of honeycomb liquid-cooled battery module is established, and the heat transfer behavior under different central angle of channel, coolant flow rates, and temperatures of the battery module at different ambient temperature are researched. The study can provide guidance for thermal management for large capacity cylindrical batteries.

Model establishment and validation

Geometric model

The total number of lithium batteries is 36 (6×6), all of which are 18650-type cylindrical lithium batteries. Batteries are placed in cylindrical holes. The whole battery module is 171 mm long, 171 mm wide, and 65 mm high. Figures 1 and 2 shows the battery module and a channel-battery unit.

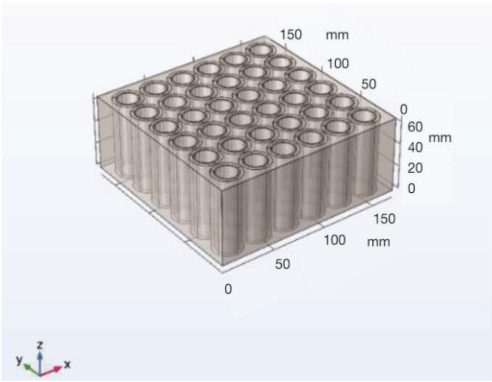

Figure 1. Honeycomb lithium battery module

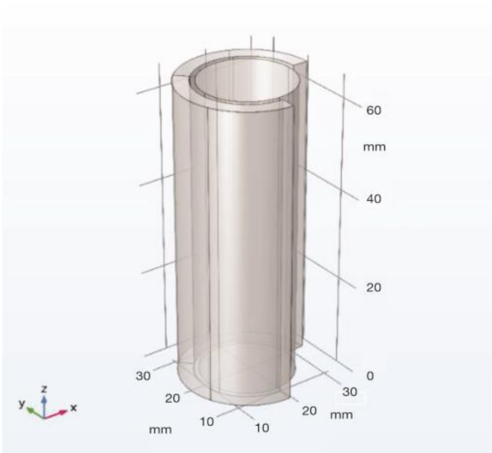

Figure 2. Channel-battery unit

Each liquid-cooling channel is made up of two annular cylinders (135°) with a width of 3 mm, an interval of 1 mm between batteries and cooling channels. The cooling channel's height equals the battery's height, and 36 channels surround each battery. The flow direction of coolant in the two flow channels is opposite. Figures 3 and 4 show the inlet of cooling fluid.

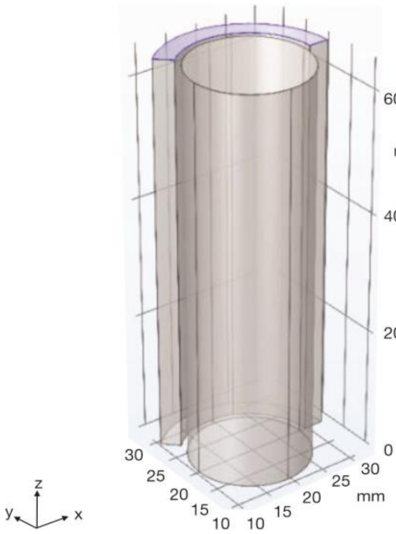

Figure 3. The inlet of cooling fluid (Blue boundary)

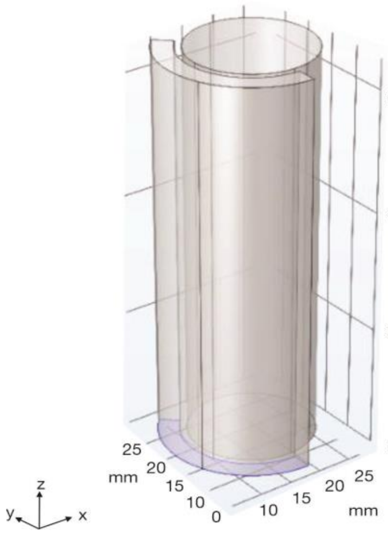

Figure 4. The inlet of another cooling fluid (Blue boundary)

Mathematical model

Thermodynamic model

The total heat production, Q, inside the battery comprises four parts: reaction heat, Q_r, polarised heat, Q_p, Ohmic heat, Q_j, and decomposition heat, Q_s [31]. The heat production of each heat-producing reaction varies at different operating temperatures. When the battery is in the normal operating temperature range, the battery's decomposition heat is negligible. However, if the battery temperature exceeds 353.15 K, the decomposition heat will increase dramatically, leading to battery failure, even an explosion. Therefore, to simplify calculation of the battery's normal operation, the battery's total heat production can be expressed:

$$Q = Q_r + Q_p + Q_j \tag{1}$$

The internal resistance Joule heat during battery charging and discharging is an irreversible reaction heat. The internal resistance mainly consists of Ohmic internal resistance and polarized internal resistance. The heat production formula is:

$$Q_j + Q_p = I\left(U_o - U\right) = I^2\left(R_j + R_p\right) \tag{2}$$

where Q_j [J] is the Ohmic heat, Q_p [J] – the polarised heat, I [A] – the operating current, the nominal current of the battery is 3.4 A, U_o [V] – the battery open-circuit voltage, U [V] – the operating voltage, R_j [Ω] – the Ohmic internal resistance, and R_p [Ω] – the polarized internal resistance.

According to the theory of chemical thermodynamics and the theory of external work, the reaction heat is:

$$Q_r = -IT\frac{\partial U_o}{\partial T} \tag{3}$$

where Q_r [J] is the reaction heat, I [A] – the same as in eq. (2), T [K] – the battery's temperature, U_o [V] – the same as in eq. (2), and $\partial U_o/\partial T$ [VK^{-1}] – the entropy-thermal coefficient of the battery.

In this study, use the experimental validated rate of heat generation during discharging established by [30]:

$$q = \frac{I}{V_b}\left\{I\left[R_j\left(T,SOC\right)+R_p\left(T,SOC\right)\right]+T\frac{\partial U_o}{\partial T}\left(T,SOC\right)\right\} \tag{4}$$

where q [Wm^{-3}] is the single battery's heat generation rate, I [A] – the same as in eq. (2), V_b [m^3] – the battery volume, T [K] – the same as in eq. (3), U_o [V] – the same as in eq. (2), $\partial U_o/\partial T$ [VK^{-1}] – the same as in eq. (3), SOC – the state of charge, and R_j [Ω] and R_p [Ω] are the same as in eq. (2).

If the discharge rate is 1 C, the conversion between the SOC and the discharge time can be calculated by [30]:

$$SOC = 1 - \frac{\tau}{3600} \tag{5}$$

where SOC is the state of charge and τ [s] – the discharge time.

The R_j *(T, SOC)* and R_p *(T, SOC)* are functions of independent variable as temperature and SOC. The entropy-thermal coefficient of the battery is a function of independent variable as SOC. Using the experimental data in [30], the previous functions can be obtained by MATLAB fitting. Then import the functions into COMSOL to establish the model of a single battery's heat generation rate. Figure 5 shows the three-dimensional surface of the heat generation function.

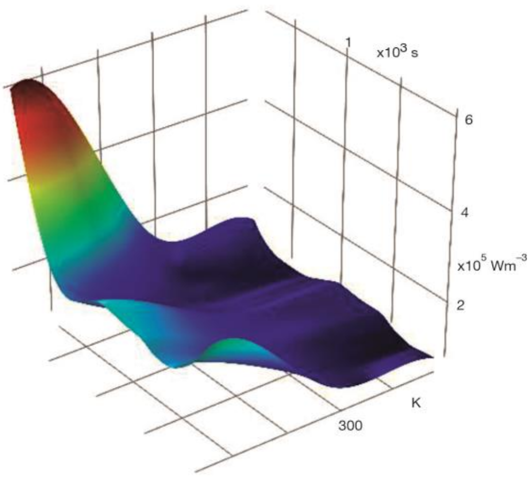

Figure 5. Heat generation function

Because batteries are an opaque system, only consider the heat conduction. For the convenience of calculation, it is assumed that the distribution of active material and heat generation is homogeneous, and the material properties are isotropic for the cylindrical lithium battery [32, 33]. The Fourier equation of batteries' heat conduction during charging and discharging in cylindrical co-ordinate system can be described:

$$\rho C_p \frac{\partial t}{\partial \tau} = \frac{1}{r}\frac{\partial}{\partial r}\left(\lambda_r r \frac{\partial t}{\partial r}\right) + \frac{1}{r^2}\lambda_\varphi \frac{\partial^2 t}{\partial \varphi^2} + \lambda_z \frac{\partial^2 t}{\partial z^2} + q \tag{6}$$

where ρ [kgm^{-3}] is the average battery density, C_p [Jkg^{-1}K^{-1}] – the average specific heat capacity of the battery, t [K] – the temperature of each microelement, τ [s] – the same as in eq. (5), λ_r, λ_ϕ, and λ_z [Wm^{-1}K^{-1}] – the coefficient of the battery's heat conduction in cylindrical co-ordinate system, and q [Wm^{-3}] – the same as in eq. (4).

Determining physical properties

The material of the battery module's main part is aluminum. The cooling fluid is liquid water. The average battery density, specific heat capacity and heat conduction coefficient of the battery can be calculated using:

$$\rho = \frac{\sum \rho_i V_i}{\sum V_i} \tag{7}$$

$$C_p = \frac{\sum \rho_i C_{p,i} V_i}{\rho \sum V_i} \tag{8}$$

$$\lambda_\phi = \lambda_z = \frac{\sum \lambda_i A_i}{\sum A_i}, \quad \lambda_r = \frac{\sum L_i}{\sum \frac{L_i}{\lambda_i}} \tag{9}$$

where ρ [kgm^{-3}] is the same as in eq. (6), ρ_i [kgm^{-3}] – the density of each layer of material in the battery, V_i [m^3] – the volume of each layer of material in the battery, C_p [Jkg^{-1}K^{-1}] – the same as in eq. (6), $C_{p,i}$ [Jkg^{-1}K^{-1}] – the specific heat capacity of each layer of material in the battery, λ_r, λ_ϕ, and λ_z [Wm^{-1}K^{-1}] – the same as in eq. (6), A_i [m^2] – the section area of each layer, L_i [m] – the thickness of each layer, and λ_i [Wm^{-1}K^{-1}] – the coefficient of heat conduction of each layer.

Table 1 shows the single battery's [30] and materials' physical properties. The physical function of liquid water comes from COMSOL materials' database.

Table 1. Physical properties of single battery and materials

Parameter	λ [Wm^{-1}K^{-1}]	ρ [kgm^{-3}]	C_p [Jkg^{-1}K^{-1}]
Lithium battery	$\lambda_\phi = \lambda_z$=29.853 λ_r = 1.473	2776.288	1075.94
Aluminum	238	2700	900
Liquid water	Varies with temperature	Varies with temperature	Varies with temperature

Initial and boundary conditions

The entire battery module's initial temperature is the same as the ambient temperature. Coolant flows in at a constant flow rate, pressures flow out at a constant pressure, and the walls are assumed to be non-slippery. The relative pressure at the coolant outlet is set to zero. The central angles of coolant channel are 135°, 155°, and 175°, respectively. Coolant flow rates are 0.6 m/s, 1.2 m/s, 1.8 m/s, and 2.4 m/s to ensure that the Reynolds number is greater than the laminar critical Reynolds number of forced convection in the tube.

The Reynolds number can be calculated by:

$$\mathrm{Re} = \frac{ul}{\nu} \tag{10}$$

where u [ms^{-1}] is the coolant's flow rate, l [m] – the channel's characteristic length, and ν [m^{2}s^{-1}] – the coolant's kinematic viscosity. Corresponding to different central angles of channel, the characteristic lengths of the channel are $5.42 \cdot 10^{-3}$, $5.47 \cdot 10^{-3}$, and $5.53 \cdot 10^{-3}$ m, respectively.

The coefficient of natural heat convection between battery module and environment is set to be 9 W/m^{2}K.

Model validation and mesh independence validation

To further validate the accuracy of the single battery's thermodynamic model, using the experimental validated values from [30] as a Benchmark and selecting the same initial values and boundary conditions. Figure 6 shows the comparison of the highest temperature of a single battery under different ambient temperatures and discharge rates.

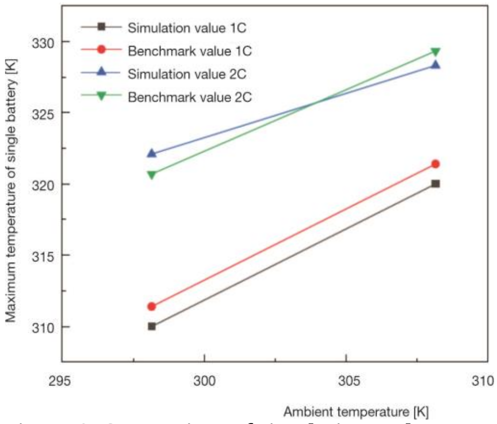

Figure 6. Comparison of simulation and Benchmark values

The ambient temperatures are 298.15 K and 308.15 K. The discharge rates are 1 C and 2 C. The error between the simulation value and Benchmark value is less than 5%, basically proving the single battery model's accuracy. It can be seen that the discharge rate has a significant effect on the heat generation characteristics of lithium batteries, and the increase in the discharge rate will increase the heat generation and temperature rise of the battery.

Furthermore, the choice of mesh number and time step might affect the simulation results. Figures 7 and 8 show the mesh number and time step independence validation of the battery module. The ambient temperature is 298.15 K, the discharge rate is 2 C, the coolant flow rate is 0.6 m/s, and the coolant temperature is 298.15 K.

From figs. 7 and 8, the maximum error is less than 3%. Therefore, to save computing resources, choose 1 s for the time step and 500,000 for the mesh number.

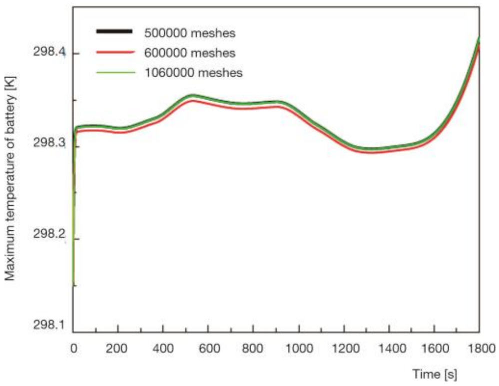

Figure 7. Mesh independence validation

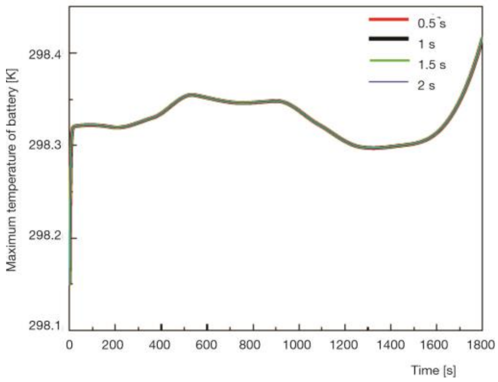

Figure 8. Time step independence validation

Discussion on heat transfer characteristics of the battery module

Cooling characteristics of the battery module at an appropriate ambient temperature

The ambient and coolant temperature are both 298.15 K and the discharge rate is 2 C. The central angle is 135°. Figure 9 shows the number of each battery. Figures 10-12 show the battery module's maximum temperature, T_{max}, maximum temperature difference, T_{diff-m}, and maximum temperature difference of each battery, $T_{\text{diff-b}}$, at different coolant flow rates. Figure 13 shows the temperature distribution of the battery module at the end of discharge.

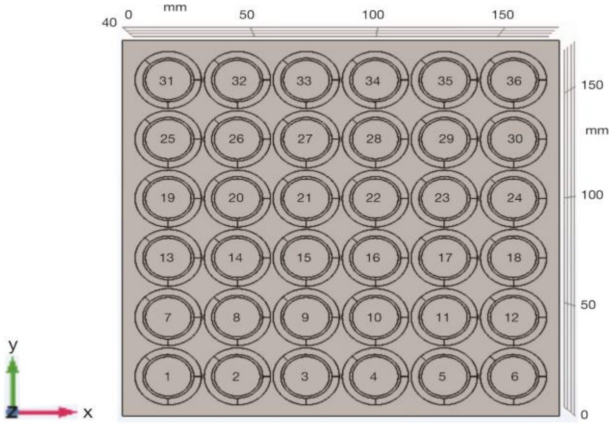

Figure 9. Number of each battery

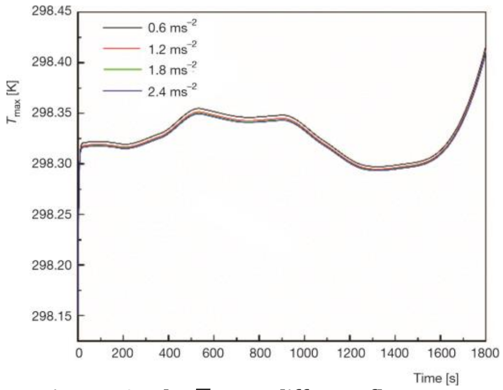

Figure 10. The $T_{\max}$ at different flow rates

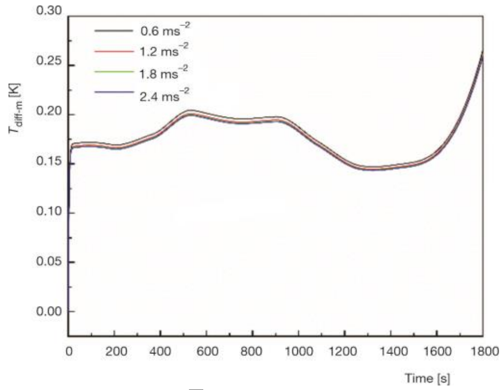

Figure 11. The $T_{\text{diff-m}}$ at different flow rates

From figs. 10 and 11, during the entire discharge process, $T_{\max}$ can always be maintained in an appropriate temperature range. And $T_{\text{diff-m}}$ does not exceed 0.3 K, indicates that the temperature distribution of the battery module is homogeneous.

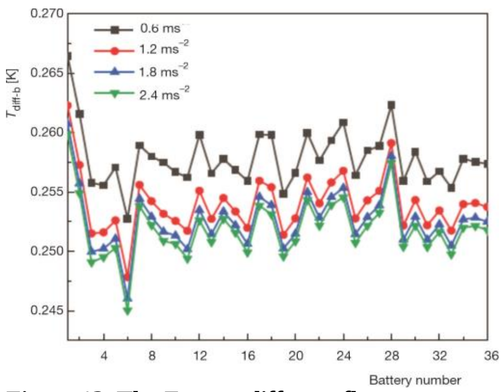

Figure 12. The $T_{\text{diff-b}}$ at different flow rates (t = 1800 s)

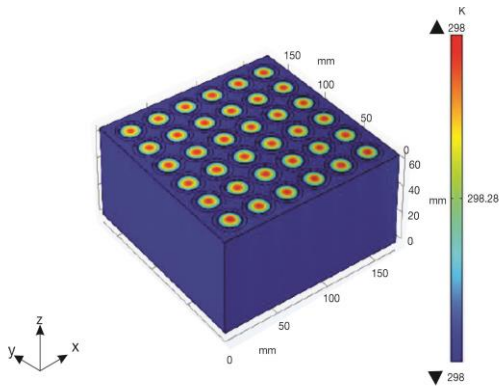

Figure 13. Temperature distribution (t = 1800 s, 0.6 m/s)

From fig. 12, T_{diff-b} is less than 0.27 K, indicates that the temperature distribution of each battery is homogeneous. Due to the one-to-one heat exchange between the batteries and the coolant channels, T_{diff-m} is approximately equal to T_{diff-b}. From fig. 13, it can be seen more directly that the temperature distribution of the battery module is homogeneous. This is also due to the one-to-one heat exchange between the batteries and the coolant channels, and the battery does not interfere with each other, which improves the heat exchange.

Cooling characteristics of the battery module at high temperature

Figure 14 shows the temperature distribution at the end of discharge. The ambient temperature is 313.15 K, the coolant temperature is 293.15 K, the coolant flow rate is 0.6 m/s, the central angle is 135°, and the discharge is 2 C.

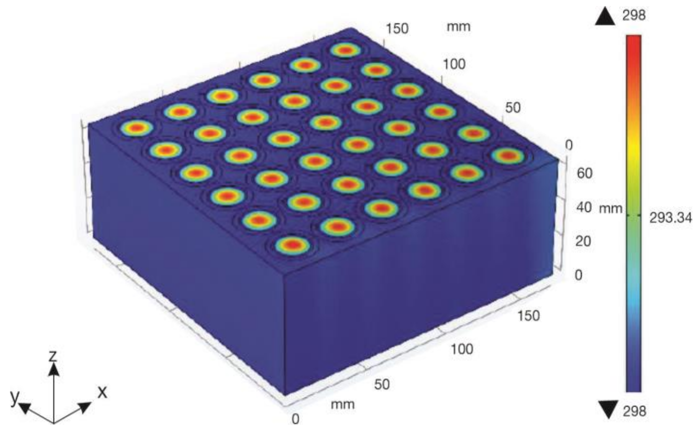

Figure 14. Temperature distribution (t = 1800 s)

The influence of coolant flow rate on cooling characteristics

The ambient temperature is 313.15 K, and the coolant temperature is 293.15 K. The discharge rate is 2 C. The central angle is 135°. Figures 15 and 16 show T_{max} and T_{diff-m} at different coolant flow rates.

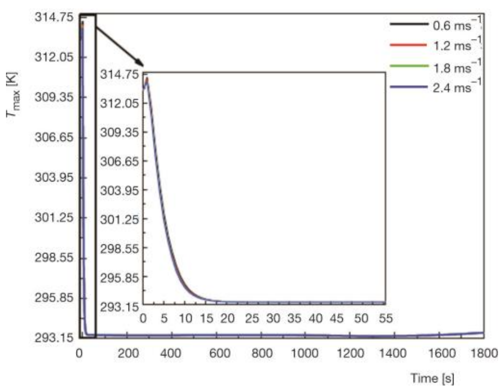

Figure 15. The T_{max} at different flow rates

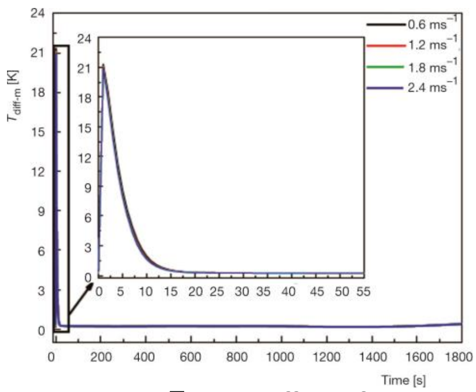

Figure 16. The T_{diff-m} at different flow rates

From fig. 15, when the coolant flow rate is constant, T_{max} presents a trend of *rising-falling-stable*. Because in the first 2 s of the discharge, the heat generation at the axial position of the battery is greater than the heat exchange, resulting in an increase in T_{max}. Then as the coolant flows, the heat generated by batteries is taken away in time, T_{max} decreases rapidly, and after about 20 seconds, it basically remains stable. For the same reason, T_{diff-m} also has the same trend.

From figs. 15 and 16, as the coolant flow rate increases, T_{max} and T_{diff-m} gradually decreases, but the change is not obvious. The flow rate increased from 0.6 m/s to 2.4 m/s, the maximum reduction values of T_{max} and T_{diff-m} are 0.8543 K and 0.8536 K, respectively. It indicates that increasing the coolant flow rate has limited improvement on the cooling effect. This is because when the flow state of coolant is turbulent, the change of thickness of laminar sub-layer caused by the increase of flow rate is small and the improvement of the heat exchange is not significantly.

The influence of coolant temperature on cooling characteristics

The ambient temperature is 313.15 K, and the coolant flow rate is 0.6 m/s. The discharge rate is 2 C. The central angle is 135°. Figures 17 and 18 show T_{max} and T_{diff-m} at different coolant temperatures.

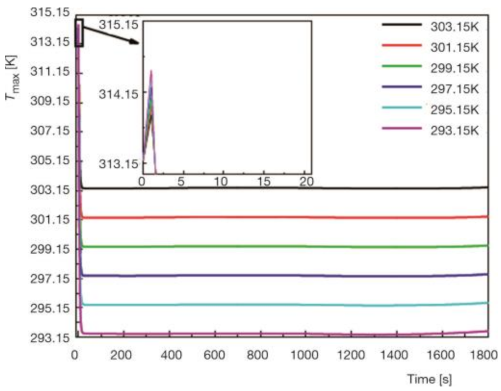

Figure 17. The T_{max} at different coolant temperatures

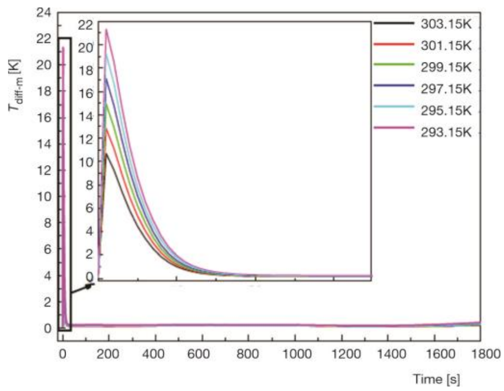

Figure 18. The T_{diff-m} at different coolant temperatures

From figs. 17 and 18, when the coolant temperature is constant, T_{max} and T_{diff-m} both presents a trend of *rising-falling-stable*. Because the heat exchange at the position of the battery near the coolant channel is stronger than the heat generation, and the heat generation at the position of the battery axis is greater than the heat exchange, T_{max} and T_{diff-m} increases rapidly in the first 2 seconds of discharge. As the coolant flows, T_{max} and T_{diff-m} gradually decrease. After about 20 seconds, the heat exchange and heat generation of the battery reach a dynamic balance, T_{max} and T_{diff-m} are basically stable. Meanwhile, the lower coolant temperature, the lower T_{max} when it is stable, but the higher T_{diff-m} in the first 10 seconds. This is because the lower coolant temperature, the greater the temperature difference and enhances heat exchange.

The influence of central angles of coolant channel on cooling characteristics

The ambient temperature is 313.15 K, and the coolant flow rate is 0.6 m/s. The discharge rate is 2 C. The coolant temperature is 293.15 K. Figures 19 and 20 show T_{max} and T_{diff-m} at different central angles of coolant channel.

Similar to figs. 15 and 16, as the center angle of the coolant channel increases, T_{max} and T_{diff-m} gradually decrease. The central angle increased from 135° to 175°, the maximum reduction values of T_{max} and T_{diff-m} are 1.595 K and 1.586 K. Compare with increasing the coolant flow rate, increasing the center angle has a more obvious effect on T_{max} and T_{diff-m}. This is because when the flow rate is constant, increasing the center angle increases the heat exchange area between the coolant channel and the battery, and enhances heat exchange.

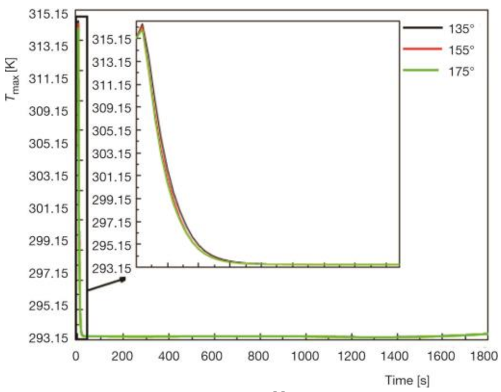

Figure 19. The T_{max} at different central angles

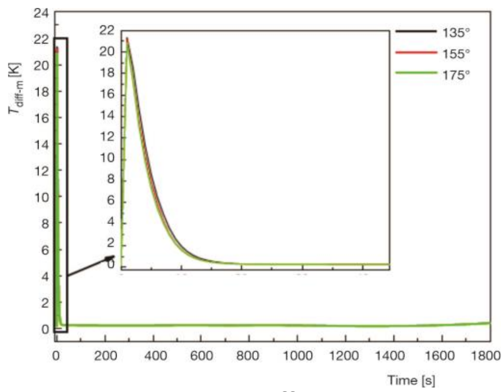

Figure 20. The T_{diff-m} at different central angles

Heating characteristics of the battery module at low temperature

According to the previous analysis in section *Cooling characteristics of the battery module at high temperature*, the heat exchange at the position of the battery near the coolant channel is greater than the heat exchange at the position of the battery axis. Therefore, the minimum temperature of the battery module, T_{min}, is selected as an index for analysing the heating characteristics of the battery module in this section. Figure 21 shows the temperature distribution at the end of discharge. The ambient temperature is 253.15 K, the coolant temperature is 303.15 K, the coolant flow rate is 0.6 m/s, the central angle is 135°, and the discharge is 2 C.

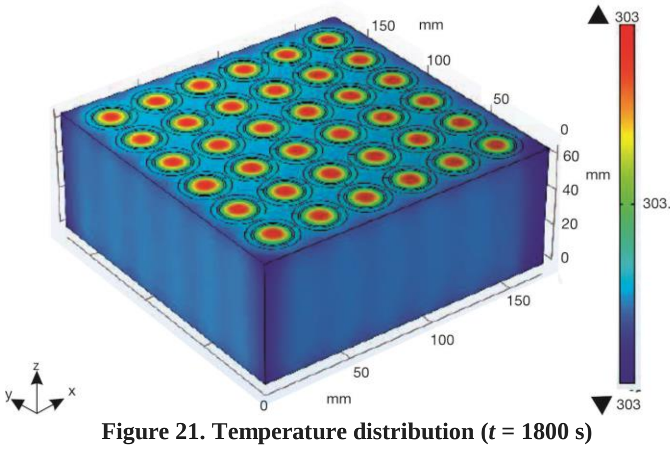

Figure 21. Temperature distribution (*t* = 1800 s)

The influence of coolant flow rate on heating characteristics

The ambient temperature is 253.15 K, and the coolant temperature is 303.15 K. The central angle is 135°. The discharge rate is 2 C. Figures 22 and 23 show T_{min} and T_{diff-m} at different coolant flow rates.

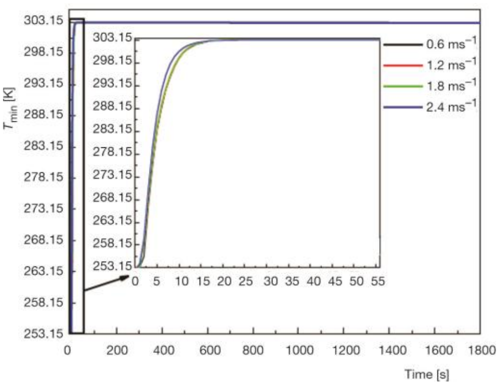

Figure 22. The T_{min} at different flow rates

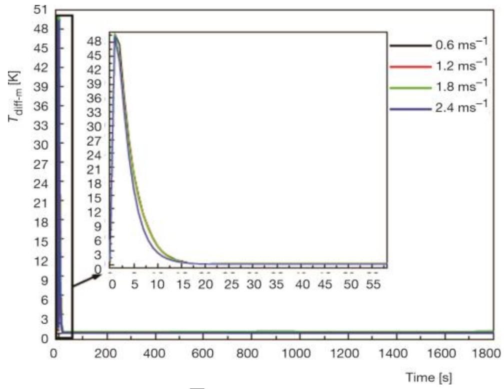

Figure 23. The T_{diff-m} at different flow rates

From figs. 22 and 23, that as the coolant flow rate increases, T_{min} gradually increases and T_{diff-m} gradually decreases. The flow rate increased from 0.6 m/s to 2.4 m/s, the maximum difference of T_{min} and T_{diff-m} are 3.815 K and 3.774 K. Compare with the cooling characteristics of the battery module, the coolant flow rate has a more obvious effect on the heating characteristics of the battery module.

The influence of coolant temperature on heating characteristics

The ambient temperature is 253.15 K, and the coolant flow rate is 0.6 m/s. The discharge rate is 2 C. The central angle is 135°. Figures 24 and 25 show T_{min} and T_{diff-m} at different coolant temperatures.

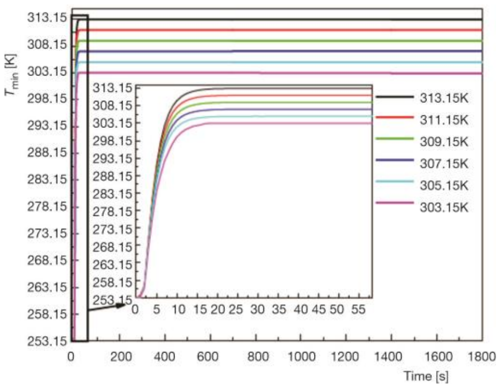

Figure 24. The T_{min} at different coolant temperatures

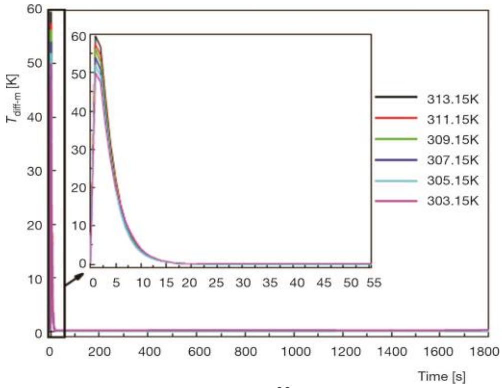

Figure 25. The T_{diff-m} at different coolant temperatures

From fig. 24, T_{min} presents a trend of *rising-stable*. As the coolant temperature increases, T_{min} also increases.

From fig. 25, T_{diff-m} presents a trend of *rising-falling-stable*. Similar to cooling characteristics, in the first 2 seconds of the discharge, T_{diff-m} rises. This is still caused by the difference in heat exchange between the position of the battery axis and the position close to the coolant channel. The difference from the cooling characteristics is that the higher coolant temperature, the higher T_{max} when it is stable, and the higher T_{diff-m} in the first 10 seconds.

The influence of coolant temperature on heating characteristics

The ambient temperature is 253.15 K, and the coolant flow rate is 0.6 m/s. The discharge rate is 2 C. The coolant temperature is 303.15 K. Figures 26 and 27 show T_{min} and $T_{diff\text{-}m}$ at different central angles of coolant channel.

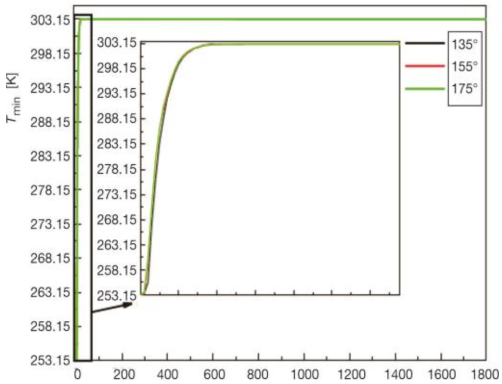

Figure 26. The T_{min} at different central angles

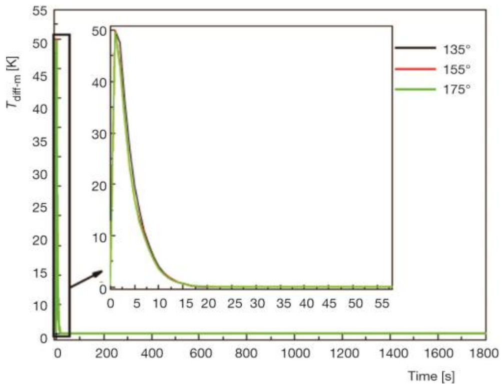

Figure 27. The $T_{diff\text{-}m}$ at different central angles

From figs. 26 and 27, as the center angle of the coolant channel increases, T_{min} gradually increases and $T_{diff\text{-}m}$ gradually decreases. The central angle increased from 135° to 175°, the maximum differennce values of T_{min} and $T_{diff\text{-}m}$ are 4.715 K and 4.710 K. Compare with increasing the coolant flow rate, increasing the center angle has a more obvious effect on T_{min} and $T_{diff\text{-}m}$. This is similar to the cooling characteristics.

Conclusion

- In an appropriate working environment, the coolant temperature is the same as the ambient temperature, and when the coolant flow rate is 0.6 m/s, the temperature of the battery module can be maintained within a appropriate temperature range without the need to reduce the coolant temperature. When the ambient temperature is 298.15 K, T_{max}, $T_{diff\text{-}m}$, and $T_{diff\text{-}b}$ are less than 298.45 K, 0.3 K, and 0.27 K respectively, which meets the requirements of the liquid cooling strategy.
- Regarding the cooling characteristics of the battery module, T_{max} and $T_{diff\text{-}m}$ are basically stable after only about 20 seconds. The T_{max} is close to the coolant temperature, and $T_{diff\text{-}m}$ is less than 0.5 K, which meets the requirements of the liquid cooling strategy.
- Regarding the heating characteristics of the battery module, similar to the cooling characteristics, T_{min} and $T_{diff\text{-}m}$ are basically stable after only about 20 seconds. The T_{min} is close to the coolant temperature, and $T_{diff\text{-}m}$ is less than 0.5 K, which meets the requirements of the liquid heating strategy.
- Regardless of heating or cooling, the honeycomb liquid-cooled lithium battery module proposed in this study not only meets the temperature difference and temperature rise requirements of engineering applications, but also basically guarantees the temperature homogeneity of each battery.
- The temperature difference has the greatest influence on the heat transfer characteristics of the battery module, followed by the heat exchange area, and the heat exchange coefficient has the least influence.

References

[1] Zhang, H., *et al*., Study on Non-isothermal Kinetics and the Influence of Calcium Oxide on Hydrogen Production during Bituminous Coal Pyrolysis, *Journal of Analytical and Applied Pyrolysis*, *150* (2020), Sept., 104888
[2] Wu, S. T., Prospect of Application of Hybrid Trains, *Transport Energy Conservation & Environmental Protection*, *15* (2019), 4, pp. 117-121
[3] Wang, Q. T., *et al*., Dynamic Thermal Modeling and Voltage Distribution Simulation for 18650-type Lithium-ion Battery Under Discharge Cycles, *Bulletin of Science and Tec.*, *36* (2020), 2, pp. 45-49
[4] Motloch, C. G., *et al*., High-power Battery Testing Procedures and Analytical Methodologies for HEV's, *SAE International Journal of Engines, 111* (2002), Jan., pp. 797-802
[5] Panchal, S., *et al*., Experimental and Theoretical Investigations of Heat Generation Rates for A Water Cooled $LiFePO_4$ Battery, *International Journal of Heat and Mass Transfer*, *101* (2016), Oct., pp. 1093-1102
[6] Li, W. Q., *et al*., Experimental Study of a Passive Thermal Management System for High-powered Lithium Ion Batteries Using Porous Metal Foam Saturated with Phase Change Materials, *Journal of Power Sources*, *255* (2014), June, pp. 9-15
[7] Zhou, Z. C., *et al*., Heat Transfer Characteristics of Oscillating Heat Pipe and its Application in Power Battery Cooling, *Chemical Industry and Engineering Progress*, *39* (2020), 10, pp. 3916-3925
[8] Zheng, F. D., *et al*., Study of Synthesized Performance Evaluation Method of Power Battery Based on The Target of Matching Battery Packs, *Systems Engineering-Theory & Practice*, *35* (2015), 2, pp. 528-536
[9] Feng, N. L., *et al*., Experimental Study on Heat Transfer Characteristics of Honeycomb Liquid Cooled Battery Module, *Automotive Engineering*, *42* (2020), 5, pp. 658-664
[10] Li, W., *et al*., A Surrogate Thermal Modeling and Parametric Optimization of Battery Pack with Air Cooling for EVs, *Applied Thermal Engineering*, *147* (2018), Oct., pp. 90-100
[11] Wang, Y., *et al*., Optimization of Liquid Cooling Technology for Cylindrical Power Battery Module, *Applied Thermal Engineering*, *162* (2019), Nov., 114200
[12] Shi, S., *et al*., Battery Thermal Management System Using Phase Change Materials and Foam Copper, *CIESC Journal*, *68* (2017), 7, pp. 2678-2683
[13] Rao, Z. H., *et al*., Experimental Investigation on Thermal Management of Electric Vehicle Battery with Heat Pipe, *Energy Conversion and Management*, *65* (2013), Jan., pp. 92-97
[14] Song, L. M., *et al*., Thermal Analysis of Conjugated Cooling Configurations Using Phase Change Material and Liquid Cooling Techniques for A Battery Module, *International Journal of Heat and Mass Transfer*, *133* (2019), Apr., pp. 827-841
[15] Chen, D. F., *et al*., Comparison of Different Cooling Methods for Lithium ion Battery Cells, *Applied Thermal Engineering*, *94* (2016), June, pp. 846-854
[16] Rao, Z. H., *et al*., Thermal management with phase change material for a power battery under cold temperatures, *Energy Sources, Part A: Recovery, Utilization, and Environment Effects*, *36* (2014), 20, pp. 2287-2295
[17] Duan, X., and Naterer, G. F., Heat transfer in phase change materials for thermal management of electric vehicle battery modules, *International Journal of Heat and Mass Transfer*, *53* (2010), 23-24, pp. 5176-5182
[18] Javani, N., *et al*., Heat Transfer and Thermal Management with PCMs in a Li-Ion Battery Cell for Electric Vehicles, *International Journal of Heat and Mass Transfer*, *72* (2014), May, pp. 690-703
[19] Lin, C. J., *et al*., Experiment and Simulation of a $LiFePO_4$ Battery Pack with a Passive Thermal Management System Using Composite Phase Change Material and Graphite Sheets, *Journal of Power Sources*, *275* (2015), Feb., pp. 742-749
[20] Nelson, P., *et al*., Modeling Thermal Management of Lithium-Ion PNGV Batteries, *Journal of Power Sources*, *110* (2002), 2, pp. 349-356
[21] Zhang, T. S., *et al*., Status and Development of Electric Vehicle Integrated Thermal Management from BTM to HVAC, *Applied Thermal Engineering*, *88* (2015), Feb., pp. 398-409
[22] Jin, L. W., *et al*., Ultra-thin Minichannel LCP for EV Battery Thermal Management, *Applied Energy*, *113* (2014), Jan., pp. 1786-1794
[23] Huo, Y. T., *et al*., Investigation of Power Battery Thermal Management by Using Mini-channel Cold Plate, *Energy Conversion and Management, 89* (2015), June, pp. 387-395

[24] Zhao, J. T., *et al*., Thermal Performance of Mini-channel Liquid Cooled Cylinder Based Battery Thermal Management for Cylindrical Lithium-ion Power Battery, *Energy Conversion and Management*, *103* (2015), Oct., pp. 157-165
[25] Qian, Z., *et al*., Thermal Performance of Lithium-Ion Battery Thermal Management System by Using Mini-Channel Cooling, *Energy Conversion and Management*, *126* (2016), June, pp. 622-631
[26] Basu, S., *et al*., Coupled Electrochemical Thermal Modelling of a Novel Li-ion Battery Pack Thermal Management System, *Applied Energy*, *181* (2016), June, pp. 1-13
[27] Zhao, C. R., *et al*., Thermal Modeling of Cylindrical Lithium-ion Battery Module with Micro-Channel Liquid Cooling, *CIESC Journal*, *68* (2017), 8, pp. 3232-3241
[28] An, Z. G., *et al*., Effect of Ethylene Glycol on Temperature Field of 18650 Power Lithium, *Chinese Journal of Power Sources*, *43* (2019), 2, pp. 244-246+249
[29] Feng, N. L., *et al*., Heat Transfer Characteristics of Honeycomb Liquid-cooled Power Battery Module, *CIESC Journal*, *70* (2019), 5, pp. 1713-1722
[30] Wang, Y. Y., Thermal Characteristics and Thermal Management Based on Phase Change Materials of Lithium Battery, M.Sc., thesis, Qingdao University of Science and Technology, Qingdao, China, 2020
[31] Huang, R. Z., *et al*., Simulation and Optimization of Temperature Homogeneity of Liquid Cooled Lithium Battery Module, *Agricultural Equipment & Vehicle Engineering, 58* (2020), 7, pp. 96-100
[32] Wang, S. X., *et al*., Simulation and Analysis of Lithium Battery Thermal Management System for Power Vehicle, *Journal of Thermal Science and Technology, 15* (2016), 1, pp. 40-45
[33] Xiong, R., *et al*., Thermo-mechanical Influence and Analysis of External Short Circuit Faults in Lithium-ion Battery, *Journal of Mechanical Engineering, 55* (2019), 2, pp. 115-125

Paper submitted: November 23, 2021
Paper revised: January 28, 2022
Paper accepted: February 3, 2022